Natural Science
ISSN 1859–1388

http://dx.doi.org/10.26459/jns.v126i1B.4101
Vol. 126, No. 1B, 2017, P. 33–42

EXPERIMENT BASED ON FUZZY LOGIC CONTROL FOR ACTIVE MAGNETIC BEARING SYSTEM

Van Sum Nguyen*

Dept. of Electronic and Telecommunication, Hue Industrial College, 70 Nguyen Hue St., Hue, Vietnam

Abstract: This study presents an intelligent control method for positioning a non-linear active magnetic bearing (AMB) system by using an emergent fuzzy logic controller (FLC). In this work, an AMB system that supports a rotating shaft without a physical contact is presented. By using a rotor dynamic model of the AMB system and electromagnetic forces of magnetic bearing the author designed an FLC for the AMB system. A closed-loop decentralized FLC for the AMB system was designed in this study. The control algorithm was numerically evaluated to construct a multiple-input and multiple-output mathematical model of the controlled system. The membership functions and rule design of FLC were based on the mathematical model of the AMB system. A current amplifier and hardware-in-loop (HIL) were used for an electromagnetic coil to generate magnetic forces suspending the rotor in the magnetic bearing. The results indicated that the system exhibits a satisfactory control performance with a low overshooting and produces improved transient and steady-state responses under various operating conditions. The proposed controller can be feasibly applied to AMB systems exposed to various external disturbances.

Keywords: intelligent control, fuzzy logic controller, active magnetic bearing

1 Introduction

Recently, active magnetic bearings (AMB) have garnered increasing attention because of their practical applications. Magnetic bearings, rather than conventional mechanical bearings, are used in applications that require reduced noise, friction, and vibration [15, 16]. Magnetic bearings are electromechanical devices that use magnetic forces to levitate a rotor without physical contact; magnetic forces are used to suspend the rotor in an air gap. AMB systems depend on reliable control of the air gap between the stator and the rotor. An AMB system is a highly non-linear inherent multiple-input and multiple-output system (MIMO). To design an AMB controller is not easy, and the simulation controller parameters are little different from the experimental controller parameters. The relationship of the rotor displacement, the current and the electromagnetic force is highly non-linear. In practice, a precise mathematical model cannot be implemented. Therefore, several non-linear control techniques have been proposed to address the non-linear dynamics of the AMB. This study proposes a method for controlling the position of the actuator by using a fuzzy logic controller (FLC). The FLCs have recently been successfully applied to numerous non-linear systems [13, 14]. Moreover, using real-time window target (RTWT) rapid control prototyping and hardware-in-loop (HIL) testing, we can quickly change and compare the parameter values. In this work, we use data acquisition (DAQ), a current am-

* *Corresponding: nvsum@hueic.edu.vn*

Submitted: 22–5–2017; Revised: 14–6–2017; Accepted: 20–6–2017

plifier, and an eddy current sensor to set up HIL testing for the AMB system. The proposed design used an FLC to control magnetic bearings and reduce the rotor displacement of the AMB system. The controller also satisfied the real-time response and stability during disturbance requirements of the control system.

2 Structure and principle of the active magnetic bearings

Many recent studies on magnetic bearings have focused on AMBs. The experimental setup used in this paper is a two-axis symmetric structure (Figure 1).

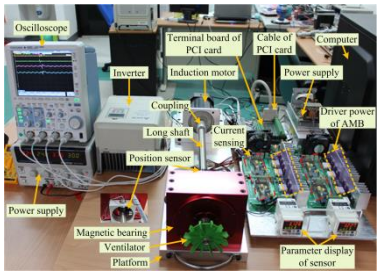

Fig. 1. Experimental design

The system is composed of a ventilator, a rotor shaft, a magnetic bearing, a coupling device, a driving motor, and other components. The drive mechanism of the AMB system includes differential driving mode power amplifiers and an analogue-digital (A/D) converter (Figure 2). Two sensors are positioned to measure the displacement of the rotor from the reference position, horizontally and vertically. The A/D converter converts the analogue signal from the position sensors into a digital signal. This signal is used as the input for the FLC, which generates a control effort according to the measurements using power amplifiers. The control signals are transformed into magnetic forces by four actuating magnets around the rotor, which hold the rotor at the reference positions. As shown in Figure 2, two pairs of electromagnetic coils are installed perpendicularly on the E-shaped stators and produce perpendicular attractive electromagnetic forces in response to dc currents. All coils installed in the AMBs have the same turns and can be considered symmetrical and uncoupled. For two degrees of freedom, two opposing electromagnets operate in the differential driving mode. As indicated in the system (Figure 2), an electromagnetic force was applied to the rotor along the x- or y-axes to keep the rotor in the centre of the AMB. The variable i_b is the bias current and i_x and i_y are control currents along the x- and y-axes, respectively. Following Schweitzer et al. [7] and Necip and Ahu [10], the total non-linear attractive electromagnetic forces along the x- and y-axes are given as follows:

$$f_{1x} - f_{2x} = k\left(\frac{\left(i_b + i_x\right)^2}{\left(x_g - x_1\right)^2} - \frac{\left(i_b - i_x\right)^2}{\left(x_g + x_1\right)^2}\right) \tag{1}$$

$$f_{1y} - f_{2y} = k\left(\frac{\left(i_b + i_y\right)^2}{\left(y_g - y_1\right)^2} - \frac{\left(i_b - i_y\right)^2}{\left(y_g + y_1\right)^2}\right) \quad (2)$$

where f_{2x}–f_{1x} and f_{1y}–f_{2y} are electromagnetic forces of the magnetic bearings along the x- and y-axes, respectively; x_1 and y_1 are rotor displacements along the x- and y-axes; k is the electromagnet constant. In this AMB system, the coil on the x- and y-axes circulates the same bias current (i_b) because the nominal air gaps along the x- and y-axes are also the same ($x_g = y_g$).

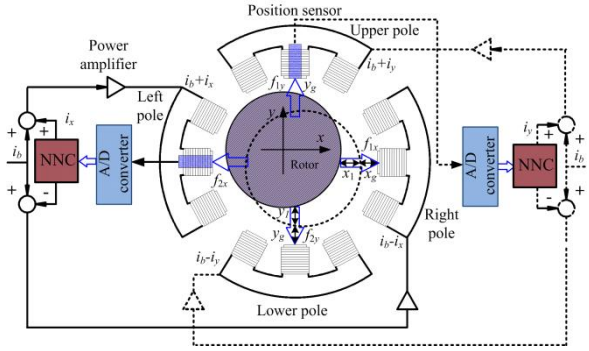

Fig. 2. Drive system of AMB

3 Rotor dynamic of the active magnetic bearing system

In this study, the rotor was assumed to be a rigid symmetric body with unbalanced uniform mass. The rotor geometry relationships with the centre of gravity (CG: x_c, y_c, z_c) in the AMB system are shown in Figure 3.

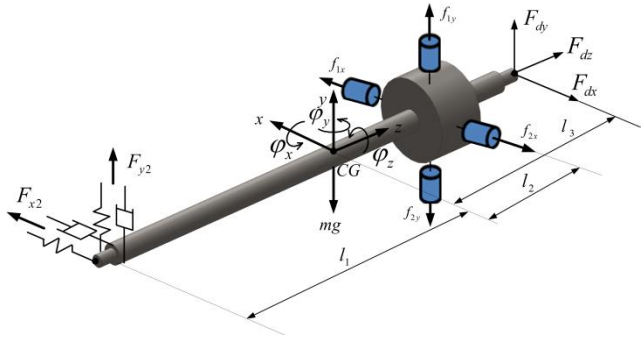

Fig. 3. Geometry relationships of rotor and AMB system

where m is the mass of the rotor; g is the gravity constant; x_c, y_c, and z_c are the coordinates of CG; F_{dx}, F_{dy}, and F_{dz} are the external disturbance forces of the rotor corresponding to the x, y, and z-axes, respectively; φ_x, φ_y, and φ_z denote the pitch, yaw, and spin angle displacements around the x-, y-, and z-axes of the rotor, respectively; and l_1 , l_2, and l_3 are the distances from CG to the flexible coupling, magnetic bearing, and external disturbances, respectively, where $l = l_1 + l_2$. The

rotor was assumed to be perfectly regulated; $\Omega = \dot{\varphi}_z$ represented the rotational speed of the rotor. The dynamic equations describing the motion of the rotor bearing system about *CG* are represented by equations (3) to (6)

$$m\ddot{x}_c = F_{x2} + F_{dx} + f_{1x} - f_{2x} \tag{3}$$

$$J\ddot{\varphi}_x + J_z\Omega\dot{\varphi}_y = l_1F_{y2} - l_2(f_{1y} - f_{2y}) + l_3F_{dy} \tag{4}$$

$$m\ddot{y}_c = F_{y2} + F_{dy} - mg + f_{1y} - f_{2y} \tag{5}$$

$$J\ddot{\varphi}_y - J_z\Omega\dot{\varphi}_x = -l_1F_{x2} + l_2(f_{1x} - f_{2x}) + l_3F_{dx}, \tag{6}$$

where J is the transverse moment of inertia of the rigid rotor around its x-axis or its y-axis; J_z is the polar mass moment of inertia of the rotor; $-J_z\Omega\dot{\varphi}_x$ and $J_z\Omega\dot{\varphi}_y$ are the gyroscopic effects when the rotor rotational speed spinning around the z-axis is Ω; and F_{x1} and F_{y1} are coupling forces. In this model, the shaft of the AMB system was fixed to the motor shaft through a coupling; therefore, the shaft displacement of the z-axis was small because it was only caused by the rotor displacement of the motor. Thus, the external disturbance forces of the z-axis rotor was approximately zero, and the external disturbance forces acting on the AMB system were exerted by two axes (x- and y-axes). Figure 4 shows the principle of unbalance force generation. The x- and y-axes are perpendicular axes in a stationary frame. The unbalanced mass forces, $\mathbf{f_d} = \begin{bmatrix} F_{dx} & F_{dy} \end{bmatrix}^T$, in the two perpendicular axes are defined using (7) and (8) [1, 4]

$$F_{dx} = m_e\varepsilon.\Omega^2\cos\Omega t \tag{7}$$

$$F_{dy} = m_e\varepsilon.\Omega^2\sin\Omega t \tag{8}$$

where m_e is the additional mass with a radius of ε in the Ωt direction.

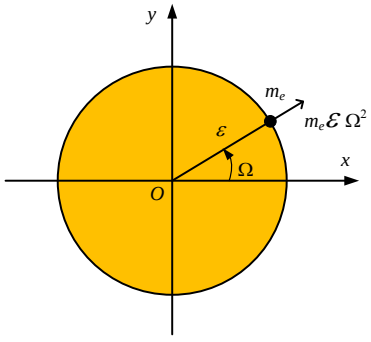

Fig. 4. Unbalance mass force

The effect of the rotor rotation was ignored, thus the flexible coupling forces corresponding to the x- and y-axes can be expressed as follows

$$F_{x2} = -d_e\dot{x}_2 - s_ex_2, \tag{9}$$

$$F_{y2} = -d_e\dot{y}_2 - s_e y_2 \tag{10}$$

where d_e is the equivalent damping coefficient; s_e is the equivalent stiffness of the coupling; and x_2 and y_2 are the shaft displacements corresponding to the x- and y-axes at the flexible coupling, respectively. Based on (1) and (2), if the four electromagnets exhibit the same static magnetic force, the non-linear electromagnetic forces can be represented using the following simplified linearized electromagnetic force [6]

$$f_{1x} - f_{2x} \cong k_{ip} i_x + k_{dp} x_1, \tag{11}$$

$$f_{1y} - f_{2y} \cong k_{ip} i_y + k_{dp} y_1, \tag{12}$$

where k_{ip} and k_{dp} are the position and current stiffness parameter of the magnetic bearing, respectively; x_1 and y_1 are the shaft displacements at the magnetic bearing. The system equations for the designed controller indicate the displacements at the locations of the flexible coupling and magnetic bearing. In addtition, because the rotor was assumed to be rigid and the displacement from the desired position was assumed to be small, the relationships between the shaft positions (x_1, x_2, y_1, y_2) and CG (x_c, y_c, z_c) are reflected as follows

$$x_c = \frac{l_1 x_1 + l_2 x_2}{l} \tag{13}$$

$$y_c = \frac{l_1 y_1 + l_2 y_2}{l} \tag{14}$$

$$\varphi_x = \frac{x_2 - x_1}{l} \tag{15}$$

$$\varphi_y = \frac{y_2 - y_1}{l} \tag{16}$$

The differential equation for a rigid rotor with its degrees of freedom transformed into bearing coordinates with displacement matrix output $\mathbf{X_c} = \begin{bmatrix} x_1 & x_2 & y_1 & y_2 \end{bmatrix}^T$ and input vector $\mathbf{u_c} = \begin{bmatrix} i_x & i_y \end{bmatrix}^T$ was used to calculate the control current vector. Substituting (13) to (16) into (3) to (6), the dynamic model of the AMB system is indicated as follows

$$\mathbf{M_c}\ddot{\mathbf{X}}_\mathbf{c} + \mathbf{G_c}\dot{\mathbf{X}}_\mathbf{c} + \mathbf{K_{ds}}\mathbf{X_c} = \mathbf{K_{is}}\mathbf{u_c} + \mathbf{E}\mathbf{f_d} + \mathbf{Dg}, \tag{17}$$

where $\boldsymbol{M_c}$ is the mass matrix; $\boldsymbol{G_c}$ is the gyroscopic matrix; $\boldsymbol{K_{ds}}$ is the displacement stiffness matrix; $\boldsymbol{K_{is}}$ is the current stiffness matrix; $\boldsymbol{E}$ is the mass unbalanced external disturbance; $\boldsymbol{f_d}$ is the external disturbance vector, and $\boldsymbol{D}$ is gravity vector and defined as follows

$$\mathbf{M_c} = \begin{bmatrix} ml_1/l & ml_2/l & 0 & 0 \\ -J/l & J/l & 0 & 0 \\ 0 & 0 & ml_1/l & ml_2/l \\ 0 & 0 & -J/l & J/l \end{bmatrix}; \quad \mathbf{K_{is}} = \begin{bmatrix} -k_{ip} & 0 \\ -l_2 k_{ip} & 0 \\ 0 & -k_{ip} \\ 0 & l_2 k_{ip} \end{bmatrix} \tag{18}$$

$$\mathbf{G_c} = \begin{bmatrix} 0 & d_e & 0 & 0 \\ J_z\Omega/l & -(J_z\Omega + l_1 l d_e)/l & 0 & 0 \\ 0 & 0 & 0 & d_e \\ 0 & 0 & J_z\Omega/l & -(J_z\Omega + l_1 l d_e)/l \end{bmatrix} \tag{19}$$

$$\mathbf{K_{ds}} = \begin{bmatrix} -k_{dp} & s_e & 0 & 0 \\ -l_2 k_{dp} & -l_1 s_e & 0 & 0 \\ 0 & 0 & -k_{dp} & s_e \\ 0 & 0 & l_2 k_{dp} & l_1 s_e \end{bmatrix}; \mathbf{E} = \begin{bmatrix} -1 & 0 \\ -l_3 & 0 \\ 0 & -1 \\ 0 & -l_3 \end{bmatrix} \tag{20}$$

$$\mathbf{f_d} = \begin{bmatrix} m_e \varepsilon . \Omega^2 \cos\Omega t \\ m_e \varepsilon . \Omega^2 \sin\Omega t \end{bmatrix}; \mathbf{D} = \begin{bmatrix} 0 & 0 & m & 0 \end{bmatrix}^T \tag{21}$$

The resulting continuous time-state-space model is given in the bearing coordinates in the form

$$\dot{\mathbf{x}} = \mathbf{Ax} + \mathbf{Bu}; \quad \mathbf{y} = \mathbf{Cx} \tag{22}$$

$$\text{with } \mathbf{x} = [\mathbf{v_c} \quad \dot{\mathbf{v}}_\mathbf{c}]^T \text{ and } \mathbf{u} = [0 \quad \mathbf{u_c}]^T \tag{23}$$

$$\mathbf{A} = \begin{bmatrix} 0 & I \\ -\mathbf{M_c^{-1}K_{ds}} & -\mathbf{M_c^{-1}G_c} \end{bmatrix}; \mathbf{B} = \begin{bmatrix} 0 \\ \mathbf{M_c^{-1}K_{is}} \end{bmatrix}; \mathbf{C} = \begin{bmatrix} I & 0 \end{bmatrix} \tag{24}$$

where $\boldsymbol{x}$ is the state vector; $\boldsymbol{u}$ is the control input signal; $\boldsymbol{y}$ is the output vector; $\boldsymbol{A}$ is the state matrix; $\boldsymbol{B}$ is the input matrix; and $\boldsymbol{C}$ is the output matrix. From equations (17) to (24), it is obvious that the relationship between the current and the electromagnetic force in the AMB system is highly non-linear. For such a non-linear system, a new control method for controlling the position of the actuator by using an FLC is proposed.

4 Control system design

4.1 Fuzzy inference system

The fuzzy inference system (FIS) is a commonly used computing framework based on the concepts of fuzzy set theory, fuzzy if-then rules, and fuzzy reasoning [3, 12, 17]. Currently, the FIS has been applied in various fields such as automatic control systems, robotics, and 3–D animation systems, and has been used in analyzing a power system and identifying harmonic disturbance problems, controlling heating and cooling in commercial appliances, conserving energy, and enabling effective operations. The FIS can be referred to as a fuzzy-rules-based system, a fuzzy expert system, a fuzzy model, a fuzzy associative memory as a fuzzy system. The basic structure of an FIS consists of four conceptual components (Figure 5).

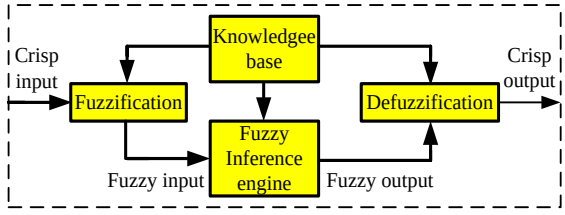

Fig. 5. Basic components of FIS

Fuzzification refers to the transformation of the crisp inputs into degrees that match linguistic values. The crisp inputs are converted to linguistic variables in the fuzzification process based on membership functions (MFs). The knowledge base consists of a rule base and a database. The rule base contains a number of fuzzy if-then rules, and the database defines the MFs of the fuzzy sets used in the fuzzy rules. The fuzzy inference engine performs inference operations on the rules. Defuzzification refers to converting the fuzzy results of the FIS into a crisp output (Figure 5). The knowledge base provides MFs and fuzzy rules required to execute the process. Crisp variables are the inputs of the system. These variables are converted to linguistic variables at the fuzzification stage and then become the fuzzy input used in the fuzzy inference engine. These fuzzy inputs can be changed to fuzzy output using the rules of the fuzzy inference engine. The fuzzy output subsequently becomes the crisp output of the system after passing through the defuzzification stage. Depending on the type of fuzzy reasoning and the fuzzy if-then rules employed, an FIS can be classified into three types: the Tsukamoto-type FIS, Mamdani-type FIS, and Takagi-Sugeno-type FIS. An in-depth analysis of each of these FISs is described in [8, 9, 18, 19].

4.2 Fuzzy logic controller design

The FLC is designed in the RTWT environment for a position-control loop. The magnetic bearing has four electromagnetic coils (a left, right electromagnetic coil for the x-axis, and a top, bottom electromagnetic coil for the y-axis), so we need two controllers for x- and y-axes of an AMB system. The controller diagram of a single-degree-of-freedom (DOF) magnetic bearing is shown in Figure 6 [5, 11]. The input of an FLC in an AMB system is the rotor displacement error (e),

and the derivative of rotor displacement error (*de*). The output of an FLC in an AMB system is current-control (*ic*). The linguistic levels of these inputs and outputs for the *x*-axis are specified (*e_x*) as *RB*: right big, *RM*: right medium, *ZE*: zero, *LM*: left medium, *LB*: left big. (*de_x*) as *N*: negative, *NS*: negative small, *ZE*: zero, *PS*: positive small, *P*: positive. (*ic_x*) as *RB*: right big, *RM*: right medium, *ZE*: zero, *LM*: left medium, *LB*: left big. Figures 7–9 show the membership functions of the inputs and outputs. The fuzzy controller rule base was composed of 25 rules for the outputs (*ic_x*) variable (Table 1) and (*ic_y*) variable (Table 2). The linguistic levels of these inputs and output for *y*-axis are specified (*e_y*) as *TB*: top big, *TM*: top medium, *ZE*: zero, *BM*: bottom medium, *BB*: bottom big. (*de_y*) as *N*: negative, *NS*: negative small, *ZE*: zero, *PS*: positive small, *P*: positive. (*ic_y*) as *BB*: bottom big, *BM*: bottom medium, *ZE*: zero, *TM*: top medium, *TB*: top big.

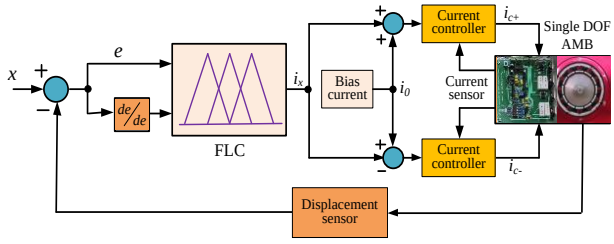

Fig. 6. FLC diagram of single DOF AMB

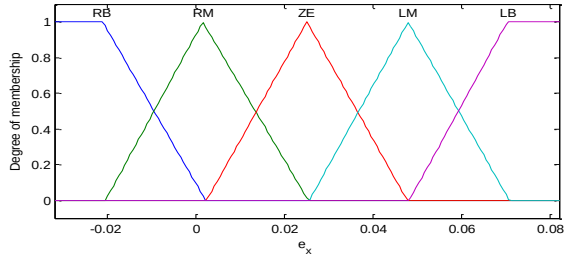

Fig. 7. Membership functions of inputs *e_x*

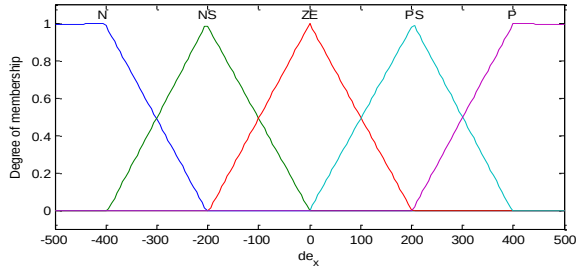

Fig. 8. Membership functions of inputs *de_x*

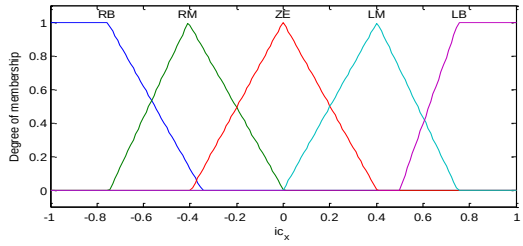

Fig. 9. Membership functions of outputs *ic_x*

Table 1. Ruless base of FLC for *x*-axis

ic_x		*e _x*				
		N	**NS**	**ZE**	**PS**	**P**
de_x	**RB**	*LB*	*LB*	*LB*	*LB*	*LB*
	RM	*LB*	*LM*	*LM*	*LM*	*LM*
	ZE	*LB*	*LM*	*ZE*	*RM*	*LB*
	LM	*RB*	*RM*	*RM*	*RM*	*RB*
	LB	*RB*	*RB*	*RB*	*RB*	*RB*

Table 2. Ruless base of FLC for *y*-axis

ic_y		*e_y*				
		N	**NS**	**ZE**	**PS**	**P**
de_y	**TB**	*BB*	*BB*	*BB*	*BB*	*BB*
	TM	*BB*	*BM*	*BM*	*BM*	*BM*
	ZE	*BB*	*BM*	*ZE*	*TM*	*BB*
	BM	*TB*	*TM*	*TM*	*TM*	*TB*
	BB	*TB*	*TB*	*TB*	*TB*	*TB*

5 Current amplifier and hardware in-loop for active magnetic bearing systems

5.1 Current amplifier

In magnetic suspension controllers, current or voltage commands are generated via the sensing of the displacement of the rotor. We can use an analogue amplifier or a switching amplifier for the AMB system. In industrial applications, switching amplifiers are used almost exclusively because their losses are considerably lower than those of analogue amplifiers. However, switching disturbances would be a problem for the controllers [2, 6].

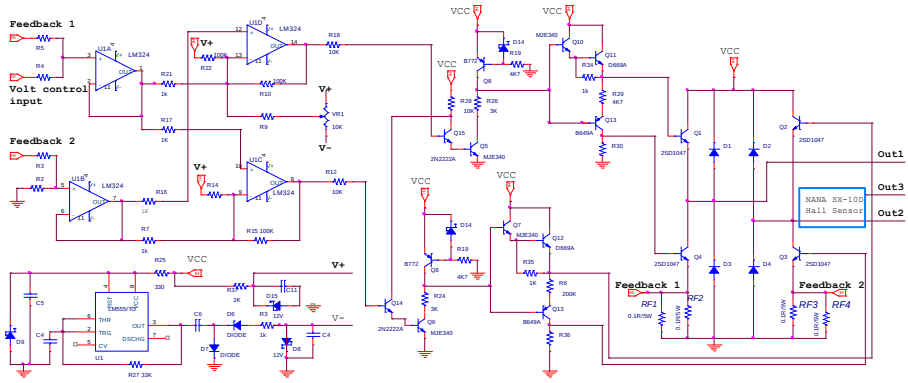

Fig. 10. Schematic of a current amplifier

In this study, using the analogue current amplifiers is a simple structure to control the AMB system. Figure 10 illustrates a schematic of a current amplifier. The output current was measured by a NANA SX–10D hall sensor. The voltage at the Out 3 terminal will connect to the PCLD 8710 for the current loop control. Table 3 shows the specifications of a current amplifier. The photograph of a current amplifier for an AMB system and the current response result are shown in Figure 11. In figure 11b, we can see that the current response is very close to the reference signal, and the setting time is about 0.01 s.

Table 3. Specifications of an analogue current amplifier test rig

No.	**Parameters**	**Values**
1	The current maximum	10 A
2	The voltage supply maximum	30 VDC
3	Current offset	0 A
4	Voltage control input (full range)	0 to 10 VDC

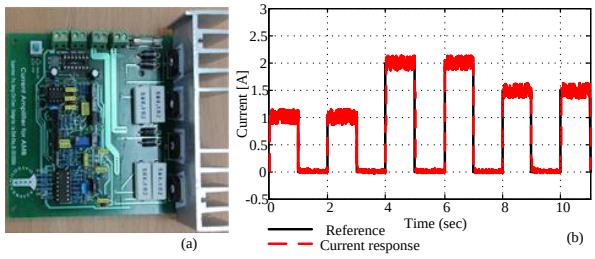

Fig. 11. (a) Photograph of a current amplifier board, (b) Current response test rig

5.2 Hardware-in-loop

Hardware-in-loop (HIL) is rapidly evolving from a control prototyping tool to system modelling, simulation, and testing. The reason that a HIL process becomes more prevalent in all industries is driven by two major factors: time and complexity. A HIL process provides an effective platform by adding the complexity of the plant under control to the test platform. The

complexity of the plant under control is included in the test and development by adding a mathematical representation of all related dynamic systems and a hardware device we want to test. The hardware device is normally an embedded system. Figure 12 displays the HIL of AMB test rig functions using the RTWT with the Matlab/Simulink models.

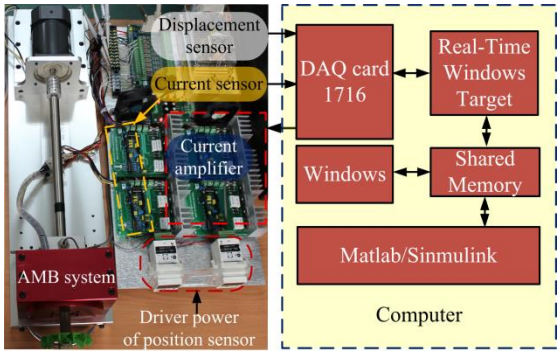

Fig. 12. Hardware-in-loop of AMB test rig functions

6 Results and discussions

The experimental setup of this study is shown in Figure 1. The laboratory setup included a horizontal shaft magnetic bearing that was symmetrical and controlled by two axes. The system was driven by an induction motor through a flexible coupling to isolate the vibration from the motor. The magnetic bearing included four identical electromagnets that were equally spaced radially around a rotor composed of laminated stainless steel (Figure 13). Each electromagnet included a coil and a laminated core composed of silicon steel.

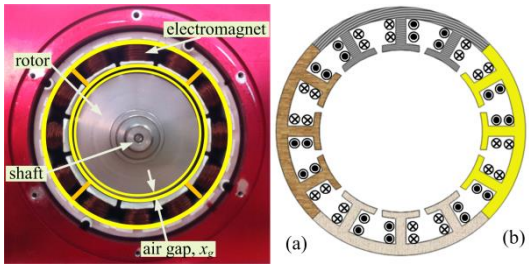

Fig. 13. Photograph of inside view (a) and layout (b) of magnetic bearing

The output current control for x- and y-axes is presented in Figure 14 with 1-A bias current. Figures 15 to 17 show the rotor displacement and orbit of the x- and y-axes at rotating speeds from 3000 rpm to 13200 rpm. At rotating speeds from 3000 rpm to 4200 rpm the rotor displacement is small (from 0.07 to 0.12 mm – Figure 16). When the rotor rotates at high speed (13200 rpm), the rotor displacement is increased by 0.16 to 0.21 mm (Figure 17), but it is still within the permitted limits of the nominal length of the air gap (x_g = 0.5 mm).

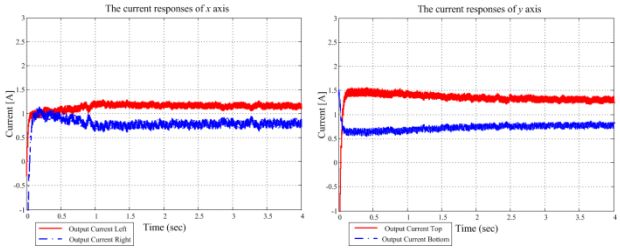

Fig. 14. Current response of x- and y-axes

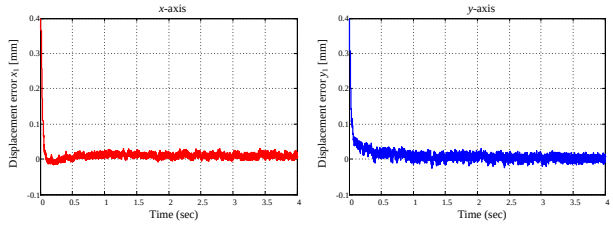

Fig. 15. Rotor displacement of x-, y-axes

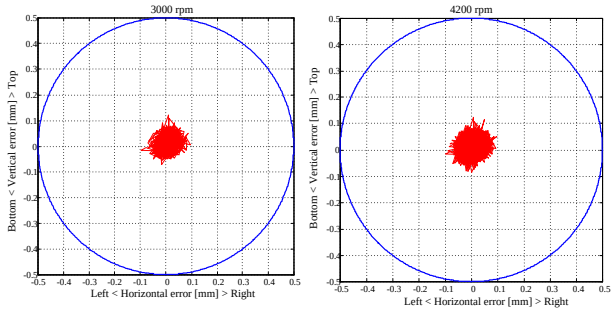

Fig. 16. Orbits of rotor center with 3000 rpm and 4200 rpm

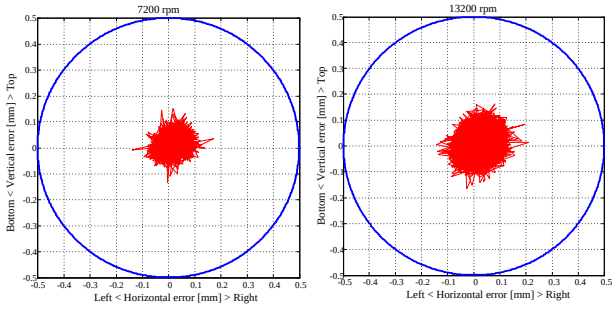

Fig. 17. Orbits of rotor center with 7200 rpm and 13200 rpm

7 Conclusions

This work develops an FLC algorithm that was applied to control the position loop of an AMB system. The results indicated that an FCL allowed the AMB system to achieve more satisfactory performance at various running rotor speeds and unbalanced masses. The results also demon-

strated that the AMB system achieved satisfactory dynamic and steady-state responses with rotor rotational speeds between 3000 rpm and 13200 rpm. This shows that the proposed controller schemes exhibit a remarkable improvement in reducing vibration in an unbalanced AMB system as well as demonstrate an efficient reduction in the shaft displacement of the rotor. This control method can be used in the AMB systems and other non-linear systems. This controller has been verified by using the position-control loop on a prototype AMB system.

References

1. Chiba, T. Fukao, O. Ichikawa, M. Oshima, M. Takemoto, and G. D. David (2005), *Magnetic bearing and bearingless drivers*, Newnes., 61–95.
2. A. Chiba, T. Fukao, O. Ichikawa, M. Oshima, M. Takemoto, D. G. Dorrell (2005), *Magnetic Bearing and Bearingless Drivers*, Elsevier: Jordan Hill, Oxford, UK, 329–342.
3. A. F. Amer, E. A. Sallam, and W. M. Elawady (2010), *Fuzzy pre-compensated fuzzy self-tuning fuzzy PID controller of 3 DOF planar robot manipulators*, Advanced Intelligent Mechatronics (AIM), 599–604.
4. A. T. Tadeo, and K. L. Cavalca (2003), *A comparison of flexible coupling models for updating in rotating machinery response*, Journal of the Brazilian Society of Mechanical Sciences and Engineering, 25 (3), 235–246.
5. F. J. Lin and R. J. Wai (2001), *Hybrid control using recurrent fuzzy neural network for linear induction motor servo drive*, IEEE Trans on Fuzzy systems, (9), 102–115.
6. G. Schweitzer, and E. H. Maslen (2009), *Magnetic bearings- Theory, design and application to rotating machinery*, Springer–Verlag.
7. G. Schweitzer, H. Bleuler and A. Traxler (1993), *Active magnetic bearings*. vdf Hochschulverlag AG, Zürich.
8. J. S. R. Jang (1993), *ANFIS: adaptive-network-based fuzzy inference system*, Systems, Man and Cybernetics, 23, (3), 665– 685.
9. K.Haisen and L. Jiang (2012), *Adaptive control for a class of non-linear system with redistributed models*, Journal of Control Science and Engineering, (2012), 1– 6.
10. M. Necip and E. H. Ahu (2007), *Variable bias current in magnetic bearings for energy optimization*, IEEE Trans on Magnetics, (43), 1052–1060,
11. M. Negnevitsky (2005), *Artificial intelligence – A guide to intelligent systems*, 2nd ed.
12. N. Wang, C. F. Hu, and W. Shi (2012), *A Mamdani fuzzy modeling method via evolution-objective cluster analysis*, Control Conference (CCC), 3470–3475.
13. P. K. Agarwal, S. Chand (2010), *Fuzzy logic control of four-pole active magnetic bearing system*, In Modelling, Identification and Control (ICMIC), The 2010 International Conference on , 533–538.
14. S. C. Chen, L.Y. Jyh, V.S. Nguyen and M. M. Hsu (2013), *A novel fuzzy neural network controller for maglev system with controlled–PM electromagnets*, Springer Journal, Lecture Notes in Electrical Engineering, (234), 551–561.
15. S. C. Chen, V. S. Nguyen, D. K. Le and M. M. Hsu (2013), *ANFIS controller for an active magnetic bearing system*, IEEE International Conference, Fuzzy Systems (FUZZ), 1–8.
16. S. C. Techn and H. C. Peter, (2012), *Article to the theory and application of magnetic bearings*, Power Electronics, Electrical Drives, Automation and Motion, (12), 1526–1534.

17. S. Kwanchai, P. Watcharin, and P. Pornjit (2011), *A hybrid of fuzzy and fuzzy self-tuning PID controller for servo electro-hydraulic system*, Industrial Electronics and Applications (ICIEA), 220–225.

18. W. L. Tung, and C. Quek (2009), *A Mamdani-Takagi-Sugeno based linguistic neural-fuzzy inference system for improved interpretability-accuracy representation*, Fuzzy Systems, 2009. FUZZ–IEEE, 367–372,

19. Y. Zhang, C. Liu, and X. Mu (2011), *Hybrid feedback stabilization of fuzzy non-linear systems*, Journal of Control Science and Engineering, (2011), 1–7.